Ultrathin Metal Silicate Hydroxide Nanosheets with Moderate Metal–Oxygen Covalency Enables Efficient Oxygen Evolution

Jiexin Zhu, Shikun Li, Zechao Zhuang, Shan Gao, Xufeng Hong, Xuelei Pan, Ruohan Yu, Liang Zhou* (ID), Lyudmila V. Moskaleva*, and Liqiang Mai* (ID)

Abstract Exploring efficient, cost-effective, and durable electrocatalysts for electrochemical oxygen evolution reaction (OER) is pivotal for the large-scale application of water electrolysis. Recent advance has demonstrated that the activity of electrocatalysts exhibits a strong dependence on the surface electronic structure. Herein, a series of ultrathin metal silicate hydroxide nanosheets (UMSHNs) $M_3Si_2O_5(OH)_4$ (M = Fe, Co, and Ni) synthesized without surfactant are introduced as highly active OER electrocatalysts. Cobalt silicate hydroxide nanosheets show an optimal OER activity with overpotentials of 287 and 358 mV at 1 and 10 mA cm^{-2}, respectively. Combining experimental and theoretical studies, it is found that the OER activity of UMSHNs is dominated by the metal–oxygen covalency (MOC). High OER activity can be achieved by having a moderate MOC as reflected by a σ*-orbital (e_g) filling near unity and moderate [3d]/[2p] ratio. Moreover, the UMSHNs exhibit favorable chemical stability under oxidation potential. This contribution provides a scientific guidance for further development of active metal silicate hydroxide catalysts.

1. Introduction

Oxygen evolution reaction (OER) is often regarded as the bottleneck of electrolytic water splitting because of its sluggish kinetics caused by multi-electron transfer process with large overpotentials.[1–3] Precious metal oxides, such as RuO_2 and IrO_2,[4,5] have been identified as benchmark OER catalysts on account of their superior catalytic activity. Unfortunately, scarcity and high-cost prohibit the broad applications of these materials. To address this issue, immense efforts have been focused on exploring new candidates.[6–10]

Recently, transition metal (TM) oxides and hydroxides, particularly cobalt-based compounds, have emerged as promising alternatives due to their earth abundance and considerable OER activities.[11–17] It has been generally accepted that a high catalytic activity can be achieved only if absorbed species bind to the catalyst surface with moderate strength.[18] Thus, further enhancing the OER activity of TM oxides and hydroxides strictly depends on optimizing their electronic structure.[19–21] Wei and co-workers have found that in an atomically thin CoOOH, the formation of $CoO_{6−x}$ with a structural distortion provokes the rearrangement of Co 3d electron population, resulting in the $t_{2g}^5 e_g^{1.2}$ configuration.[22] The hole in t_{2g} orbital and an increase in e_g filling both facilitate the adsorption of hydroxy species at active sites and the electron transfer between the surface cations and adsorbates. For oxides, such a structure–activity relationship is directly linked to metal–oxygen covalency (MOC) strength, as has been demonstrated in perovskites and spinel oxides. In octahedral coordination environment, a high catalytic activity can be achieved by having the e_g orbital filling near unity and the O p-band center located at a suitable position with respect to the Fermi level.[11,12] Because the e_g orbital interacts with the frontier orbitals of a binding OER intermediate (such as OH^-, O_2^{2-}, and O^{2-}) and has an antibonding character (M–O, σ*), its partial filling reduces the bond strength. The position of the O p-band center, on the other hand, is indicative of the degree of covalent orbital overlap between M 3d and O 2p levels. Besides, Whangbo and co-workers introduced the [3d]/[2p] (relative contribution of M 3d and O 2p orbitals to molecular orbitals) as another descriptor of the MOC.[23] As the [3d]/[2p] ratio decreases, the covalent character of metal–oxygen interaction increases. Furthermore, it has been suggested that the stronger covalency of the M–O

J. Zhu, Dr. Z. Zhuang, X. Hong, X. Pan, R. Yu., Prof. L. Zhou, Prof. L. Mai
State Key Laboratory of Advanced Technology for Materials Synthesis and Processing, Wuhan University of Technology, Wuhan Hubei 430070, China
E-mail: liangzhou@whut.edu.cn
E-mail: mlq518@whut.edu.cn
S. Li, Prof. L. V. Moskaleva
Institute of Applied and Physical Chemistry and Center for Environmental Research and Sustainable Technology, University of Bremen, Bremen 28359, Germany
Department of Chemistry, University of the Free State, PO Box 339, Bloemfontein 9300, South Africa
E-mail: moskaleva@uni-bremen.de
S. Gao
Collage of Chemistry & Chemical Engineering, Anhui University, Anhui 230000, China
Prof. L. Zhou, Prof. L. Mai
Foshan Xianhu Laboratory of the Advanced Energy Science and Technology Guangdong Laboratory, Xianhu Hydrogen Valley, Foshan Guangdong 528200, China
(ID) The ORCID identification number(s) for the author(s) of this article can be found under https://doi.org/10.1002/eem2.12155.

bond could possibly promote the charge transfer between the metal cation and the adsorbed oxygenated intermediates.

Recently, earth-abundant TM silicate hydroxides with $[MO_6]$ octahedral and $[SiO_4]$ tetrahedral motifs have been employed as efficient OER electrocatalysts.[24–27] Kang and co-workers explained how local environment of the active site in silicate hydroxides helps in stabilizing the OOH* intermediate.[25] Comparing cobalt silicate hydroxide and oxyhydroxide, they found that the lack of interlayer O–H···O bonds in the silicate hydroxide (because of the presence of silicate groups in the interlayer space) affords more flexibility to the oxygen motion of the M–OH moiety. An additional hydrogen bond is formed between the oxygen of $[SiO_4]$ tetrahedron and the hydrogen of metal–hydroxy, reducing the formation energy of the OOH* intermediate. Their groundbreaking work demonstrates that silicate hydroxides represent a family of promising OER catalysts that could become a strong alternative to precious metal oxides. Nevertheless, the intrinsic specific activity of silicate hydroxides is poorly understood up to now. The lack of fundamental understanding on OER mechanism and a meaningful activity descriptor hamper the development of highly efficient metal silicate hydroxide electrocatalysts.

In this work, we uncover the correlation between the electronic structure of metal silicate hydroxides and their OER catalytic activity through combined experimental and theoretical studies. A series of ultrathin metal silicate hydroxide nanosheets with various filling of the d shell are synthesized by a surfactant-free one-step hydrothermal method. Benefited by the rapid precipitation and ultrathin nature, oxygen-deficiency is formed on the surface of nanosheets, resulting in tunable MOC. Among the investigated compounds, including Fe, Co and Ni silicate hydroxides, the cobalt silicate hydroxide with well-suited e_g filling exhibits the highest OER activity. The theoretical calculations further demonstrate that the cobalt silicate hydroxide possesses moderate $[3d_{z^2}/2p]$ and $[3d_{x^2-y^2}/2p]$ ratio which is closely related to MOC. Besides, all the silicate hydroxide samples show favorable chemical stability under oxidation potential. This work highlights the significance of surface electronic structure and establishes the relationship between the MOC and OER activity of metal silicate hydroxide, which provides a scientific guidance for further development of active metal silicate hydroxide catalysts.

2. Results and discussion

2.1. Characterization of UMSHNs

To achieve more unsaturated ligand sites, which are likely to serve as active sites, three TM (Fe, Co, and Ni) silicate hydroxide nanosheet samples have been synthesized through a simple one-step hydrothermal method. The surfactant-free synthesis makes the active sites on the surface of the nanosheets fully exposed. Metal silicate hydroxides show a typical layered structure: each layer is comprised of an edge-sharing $[MO_2(OH)_4]$ sublayer and a corner-sharing $[SiO_4]$ sublayer, as illustrated in **Figure 1**a.[28] Owing to the rapid precipitation, the obtained silicate hydroxides lack long-range ordering, and the oxygen-deficient octahedra are formed on the surface, which leads to further splitting of the metal $3d$ energy levels.[12,29] Representative transmission electron microscope (TEM) images indicate that the prepared cobalt silicate hydroxide (CoSHN, Figure S1a, Supporting Information), iron silicate hydroxide (FeSHN, Figure S1b, Supporting Information), and nickel silicate hydroxide (NiSHN, Figure S1c, Supporting Information)

possess a similar nanosheet morphology. Selected area electron diffraction (SAED, Figure S1d–f, Supporting Information) and X-ray diffraction (XRD, Figure S2, Supporting Information) patterns indicate the as-prepared samples can be generally indexed to the orthorhombic crystal phase, despite the weak intensities of the diffractions. High-resolution TEM images (Figure 1b and Figure S3, Supporting Information) reveal that the as-prepared UMSHNs possess local orderings but lack long-range ordering as previously reported.[25] In addition, Fourier transform infrared (FT-IR) (Figure S4, Supporting Information) spectra also verify the characteristic local environment of the silicate hydroxides. The peaks at 3630–3550 cm^{-1} and 660–650 cm^{-1} correspond to the ν_{OH} vibration mode and superimposition of δ_{OH} vibration of M–OH group, while the peaks at 1010–1000 cm^{-1} and 460–450 cm^{-1} are attributed to the ν_{Si-O} vibration mode and asymmetric Si–O bending vibration.[30] The energy-dispersive X-ray (EDX) (Figure 1c, and Figures S5 and S6, Supporting Information) elemental mappings confirm the existence and uniform distribution of TM (M=Co, Fe, Ni), Si, and O elements. The high-resolution X-ray photoelectron spectroscopy (XPS) (Figure S7, Supporting Information) spectra of Co 2p, Fe 2p, and Ni 2p show 2$p_{1/2}$ and 2$p_{2/3}$ components for Co^{2+}, Fe^{2+}, and Ni^{2+}, respectively.[31,32] Atomic force microscope (AFM) images (Figure 1d, e and Figure S8, Supporting Information) demonstrate the ultrathin structure of UMSHNs, which have a thickness of <10 nm, corresponding to about 10 times of the unit cell parameter c (0.74 nm). Moreover, due to the ultrathin nature, the UMSHNs remain well-dispersed in aqueous solution for at least one month, as confirmed by TEM images and the Tyndall light scattering under laser irradiation (Figure 1f and Figure S9, Supporting Information).[33]

2.2. Electrocatalytic Properties of UMSHN Toward OER

The intrinsic OER activity of the metal silicate hydroxides containing typical metal ions (Co, Fe, and Ni) is explored by cyclic voltammetry (CV) with and without iR correction (**Figure 2**a and Figure S10, Supporting Information). To avoid the influence of trace amount of Fe on the activity of CoSHN and NiSHN, we have suspended Ni(OH)$_2$ powder in electrolyte to absorb the Fe-containing impurities.[34] The CoSHN supported on glassy-carbon electrode (GCE) exhibits the highest OER activity among the considered UMSHNs. Notably, the recorded overpotential (η) required to reach an OER current density of 1 mA cm^{-2} for CoSHN is 287 mV with a standard deviation of 3 mV, indicating a superior catalytic activity compared with the other electrodes (313 mV for FeSHN and 336 mV for NiSHN). It is worth noting that at a current density of 10 mA cm^{-2}, the CoSHN shows an overpotential of only 358 mV, surpassing that of commercial RuO$_2$ (377 mV) (Figure S11, Supporting Information). The corresponding Tafel slopes of CoSHN, FeSHN, NiSHN, and RuO$_2$ are 58.6, 66.5, 74.5, and 110.0 mV dec^{-1}, respectively (Figure 2b). Because the catalytic reaction primarily involves the surface atoms, it is more suitable to take the surface area of the catalysts as a reference rather than that of GCE, although not all surface sites are electrochemically active.[35] The intrinsic kinetic current density for OER normalized to the surface areas of the catalysts, which are measured by N$_2$ sorption (Figure S12, Supporting Information), is shown in Figure 2c. This further confirms the reliability of the activity trend by our electrochemical measurement. The overpotentials and Tafel slopes of all samples are comparable to those of previously reported single metal oxide-based OER electrocatalysts (Table S1, Supporting Information).
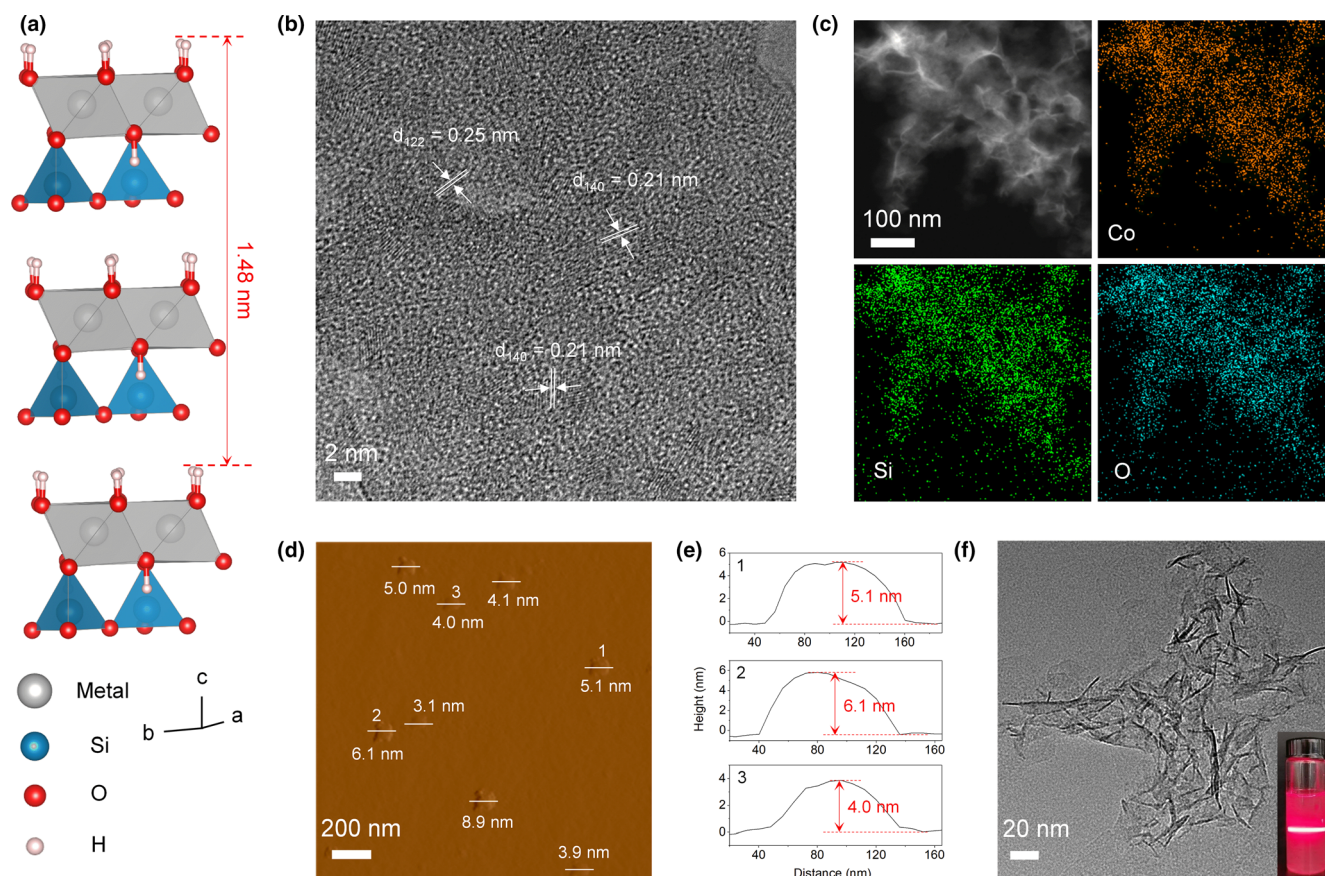
Figure 1. a) Crystal structure of silicate hydroxide. b) High-resolution TEM images of CoSHN. c) EDX elemental mappings of Co, Si, O. d,e) AFM image and the corresponding height profiles (the numbers from 1 to 3 in e correspond to the numbers from 1 to 3 in d). f) TEM image of CoSHN; The inset shows the Tyndall light scattering of CoSHN in an aqueous solution.

Further, we measured the double-layer capacitance (C_{dl}), which scales approximately with the effective electrochemical surface area (ECSA, Figure 2d and Figure S13, Supporting Information). The results reveal that the C_{dl} of CoSHN (0.371 mF cm$^{-2}_{BET}$) is close to the values determined for FeSHN (0.400 mF cm$^{-2}_{BET}$) and NiSHN (0.502 mF cm$^{-2}_{BET}$), suggesting the difference in activity rest with the inherent electronic structure rather than the increase of surface sites. The outstanding electrocatalytic activity of CoSHN is also evidenced by the high turnover frequency (TOF, 188.5 h^{-1} at 1.6 V vs RHE), which is remarkably larger than that of FeSHN (99.7 h^{-1} at 1.6 V vs RHE), NiSHN (24.8 h^{-1} at 1.6 V vs RHE) (inset in Figure 2c). From all the activity tests, the CoSHN exhibits the highest OER activity (Figure 2e). Apart from the activity, the robustness and durability are also essential factors for the catalyst. As shown in Figure 2f, the potential of the three electrocatalysts shows trivial change under a constant j = 10 mA cm^{-2} over 120 min, suggesting the absence of structural degradation on the surface of silicate hydroxides during test.

2.3. Correlation between e_g filling and OER activity of UMSHNs

To clarify the origin of OER activity variation in metal silicate hydroxides, electron spin resonance (ESR) and temperature-dependent magnetic susceptibility (M–T) measurements have been conducted to study the coordination environment, spin structures, and e_g occupancy of UMSHNs. All three samples possess a typical ESR signal centered at $g = 2.004$ (Figure S14, Supporting Information), which corresponds to oxygen vacancies,[36] the presence of which may result in further splitting of t_{2g} and e_g orbitals.[12] By fitting the temperature dependence of susceptibilities derived from the magnetizations through Curie–Weiss law, one can obtain the effective magnetic moment μ_{eff} (Figure 3a).[9] Since Co^{2+} possesses a high-spin state (HS: $t_{2g}^5 e_g^2$) and a low-spin state (LS: $t_{2g}^6 e_g^1$), the calculated μ_{eff} of 2.98 μ_B for the CoSHN translates to 5% Co^{2+} ions in HS and 95% in LS state, which corresponds to the average e_g filling of $e_g^{\sim 1.05}$ (Figure 3b). For the Fe^{2+} ions, in principle, three spin states are possible: HS ($t_{2g}^4 e_g^2$), intermediate spin state (IS: $t_{2g}^5 e_g^1$), and LS ($t_{2g}^6 e_g^0$). However, the IS has been rarely reported, while the mixtures of HS and LS are more favorable.[37,38] The μ_{eff} of 2.79 μ_B for the FeSHN can be decomposed into 32.5% HS and 67.5% LS, resulting in the $e_g^{\sim 0.65}$ configuration. Ni^{2+} ions have an electronic configuration 3d^8, corresponding to the $t_{2g}^6 e_g^2$ configuration and an e_g filling of 2.0. As shown in Figure 3c, partial electron transfers from the t_{2g} orbital to e_g orbital occur in Co^{2+} and Fe^{2+}. The created hole in the t_{2g} orbitals is believed to facilitate the adsorption of hydroxyl group on the active O sites to form adsorbed OOH by enhancing the electrophilicity of the reactive O centers.[22] The metal 3d orbitals of e_g symmetry have a σ^* antibonding character; therefore, their partial occupancy weakens the M–O bond. Thus, the CoSHN possesses a
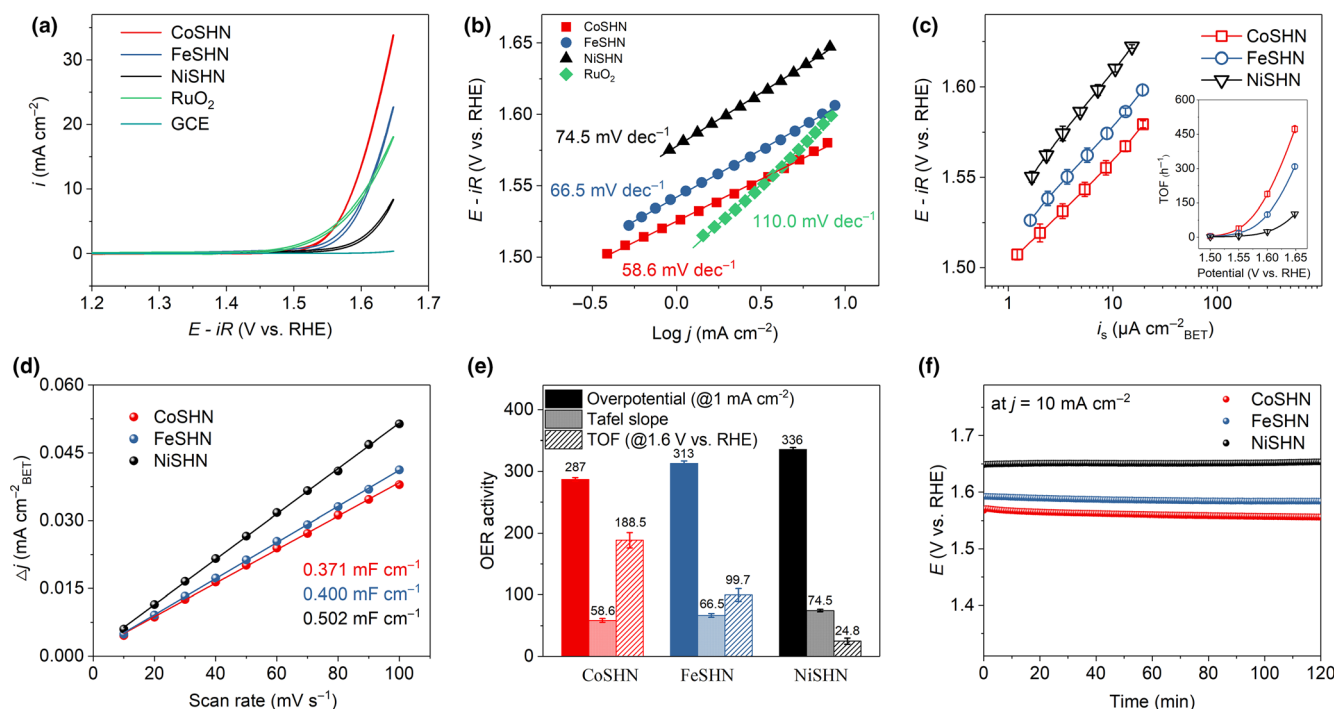
Figure 2. a) CV curves of UMSHNs, GCE, and commercial RuO_2 in O_2-saturated 1.0 M KOH. b) The corresponding Tafel plots. c) Intrinsic OER activities obtained from the currents in the backward scans and normalized by the true surface area and the inset shows TOF of UMSHNs. d) Δj at 1.175 V versus RHE as a function of the scan rate to evaluate C_{dl}. e) The summary of OER activity of UMSHNs. f) Long-term stability of CoSHN, FeSHN, and NiSHN at $j = 10$ mA cm^{-2} for 120 min.

moderate MOC, while the MOC is stronger in FeSHN and weaker in NiSHN. The relationship between the e_g filling and OER activities exhibits a volcano shape and hence the CoSHN with an e_g filling of 1.05 shows the highest OER activity among UMSHNs (Figure 3d). As a result of an e_g filling of 2.0 which is significantly far away from the optimal value, the NiSHN shows the poorest OER activity, followed by FeSHN. A series of previously reported spinel oxides are also plotted in Figure 3d, further proving the UMSHNs conform to the volcanic rule of e_g filling.[39] This observation indicates that the optimal activity of CoSHN is associated with the moderate MOC derived from the optimal e_g filling.

2.4. Correlation Between the Calculated Energy Band and OER Activity of UMSHNs

Our finding is further supported by density functional theory (DFT) calculations. Obviously, the density of states (DOS) of metal silicate hydroxides shows a comparatively small band gap, indicating a semiconductor character (Figure S15, Supporting Information). Additionally, the respective Co 3d and Fe 3d partial densities of states (PDOS) of CoSHN and FeSHN show broader peaks than the Ni 3d peaks of NiSHN (Figure S16, Supporting Information). This demonstrates that CoSHN and FeSHN bear a higher degree of electron delocalization than NiSHN, resulting in an accelerated electron transfer. Similar conclusions are obtained when inspecting the DOS in the specific M 3d PDOS region close to the Fermi level where CoSHN and FeSHN possess a higher amplitude of 3d peaks than NiSHN (Figure S17, Supporting

Information). A recent study suggested that the [3d]/[2p] ratio as a measure of the degree of covalent bonding in the metal–oxygen bonds.[23] This descriptor appears to be influencing the OER activities. It is important to highlight that in an octahedral coordination environment, the e_g orbitals (including $3d_{z^2}$ and $3d_{x^2-y^2}$) of the TM have a stronger overlap with the oxygen 2p orbitals (σ type bonding) than t_{2g} orbitals (weak π type bonding).[11] Therefore, we specifically focus on the e_g orbitals, which participate in the M–O σ bonding. As can be inferred from **Figure 4**a,b, the CoSHN exhibits a moderate relative contribution of Co $3d_{z^2}$ and Co $3d_{x^2-y^2}$ orbitals and O 2p orbitals to the σ type bonding. The smaller the [3d]/[2p] ratio the higher the covalency of the M–O bond. Thus, the Fe binds to oxygen too strongly in FeSHN, while the Ni binds to oxygen too weakly in NiSHN, whereas the binding strength between Co and O is optimal, thus yielding the best activity. The relation between the $[3d_{z^2}/2p]$ or $[3d_{x^2-y^2}/2p]$ ratio and the OER catalyst activity is compared in terms of the potential required to provide a specific current of 10 μA cm$^{-2}_{BET}$ (Figure 4c and Figure S18, Supporting Information). The optimal OER activity of silicate hydroxide can be achieved in compounds with moderate $[3d_{z^2}/2p]$ and $[3d_{x^2-y^2}/2p]$ ratio, resulting in an appropriate MOC.

2.5. Qualitative Assessment of MOC

To further support that the OER activity of UMSHNs is governed by the degree of MOC, O K–edge X-ray absorption (XAS, inset in Figure 4d) has been performed. The prepeak around 527 eV reveals a major excitation from the O 1s orbital to unoccupied M 3d–O 2p orbitals and the
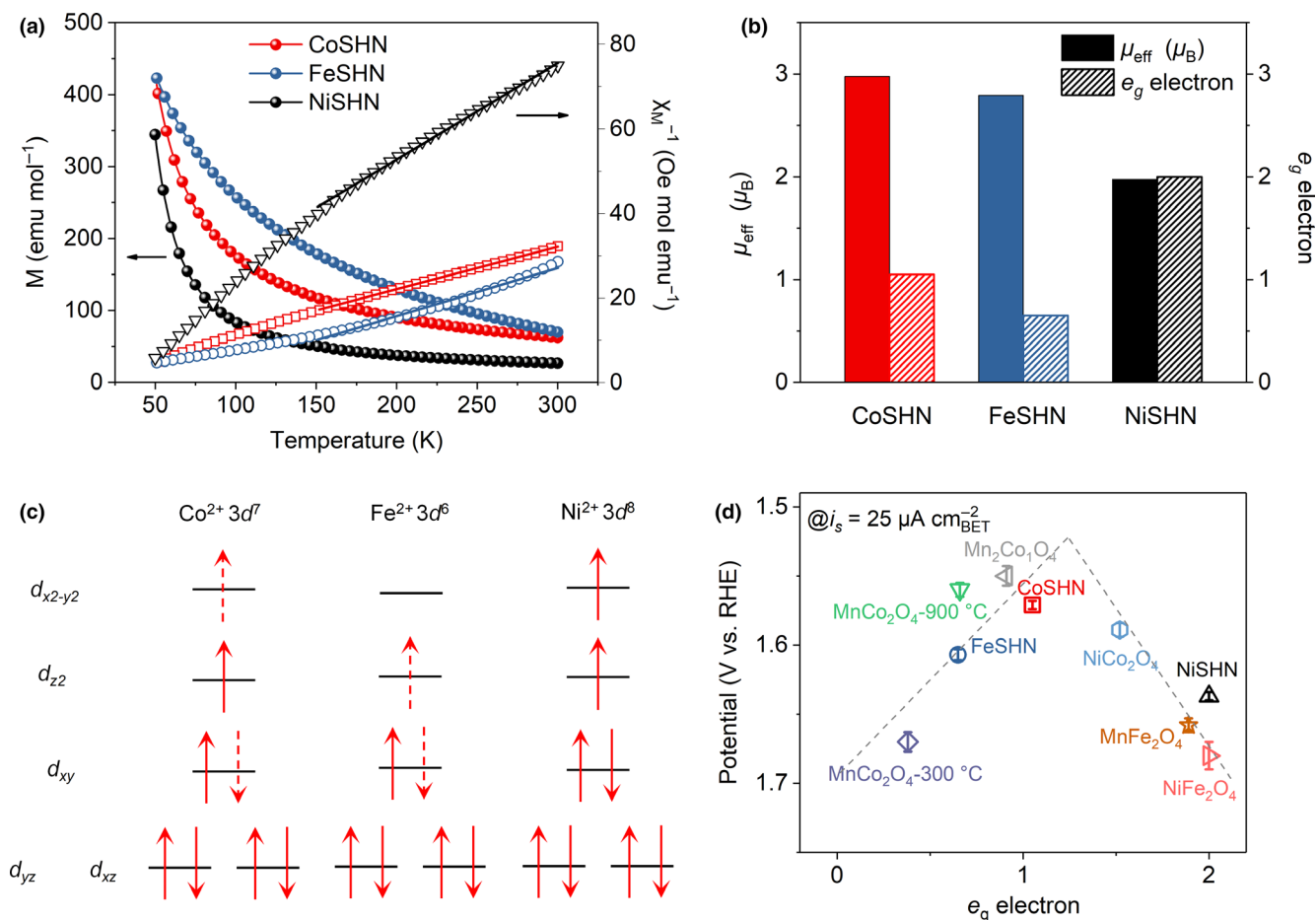
Figure 3. a) Temperature-dependent magnetization under $H = 2$ kOe and the temperature-dependent inverse susceptibilities for all the UMSHN samples. The solid lines are the fitting results by a Curie–Weiss law:$\chi = C/(T - \Theta)$ above 150 K (C, Curie constant; Θ, Curie–Weiss temperature). b) The calculated effective magnetic moment and e_g filling of UMSHNs. c) Schematic representation of e_g and t_{2g} filling of UMSHNs. d) Comparison of the iR-corrected potential at 25 µA cm^{-2} versus the e_g electron occupancy of UMSHNs and various spinel oxides from reference [35].

intensity permits quantification of the covalent character of the bond between metal and oxygen. Clearly, as the $[3d_{z^2}/2p]$ and $[3d_{x^2-y^2}/2p]$ ratio decreases, the normalized intensity of the prepeak increases accordingly. More importantly, medium MOC positively affects the OER activity of UMSHNs, which agrees with the proposed OER mechanism. The conjecture is also evidenced by the onset temperature for liberating oxygen which is detected by O_2 temperature-programmed desorption (O_2-TPD) (Figure 4e). The onset temperature of O_2 desorption decreases in the row Fe > Co > Ni, indicating a weakening of the M–O bonding and correlates with both the decreasing M–O covalency and increasing e_g filling. These results further demonstrate the adsorption ability of different silicate hydroxide to oxygen intermediate and highlight the role of MOC in OER activity of UMSHNs.

2.6. Post-Catalysts Characterizations

In situ Raman can explore the structural changes of the catalyst during the reaction (Figure f–h, Figure S19, Supporting Information). In general, silicate hydroxide is medium Raman scatters and the vibrational modes of $(SiO_4)^{4-}$ produce the major Raman peaks while M–O bonds contribute weaker Raman signals. The Raman bands in the range of 1000–1400 cm^{-1} can be assigned to the bridge antisymmetric stretching vibrations of Si–O–Si and stretching vibrations of Si–O$_{terminal}$.[40,41] The peaks of Si–O–Si bridge symmetric stretching vibrations normally occur in the range of 400–800 cm^{-1}, and those from 290 to 400 cm^{-1} are attributed to the Si–O–Si and O–Si–O bending vibrations. During CV test with the potential from 1.1 to 1.6 V versus RHE, we found that the Raman peaks of the three catalysts did not change significantly, including intensity and location. As Figure S20, Supporting Information shows, no redox peak can be detected in the CV curves of UMSHNs, which means that the valence state of metal in UMSHNs may not be changed and the electron configuration can be maintained. This indicates that the metal silicate hydroxide can maintain the structural stability during the OER process and is superior to the hydroxides. Moreover, the TEM images of silicate hydroxide electrocatalysts after electrolysis show no surface reconstruction, which also confirm the stable surface morphology and structure (Figure S21, Supporting Information).
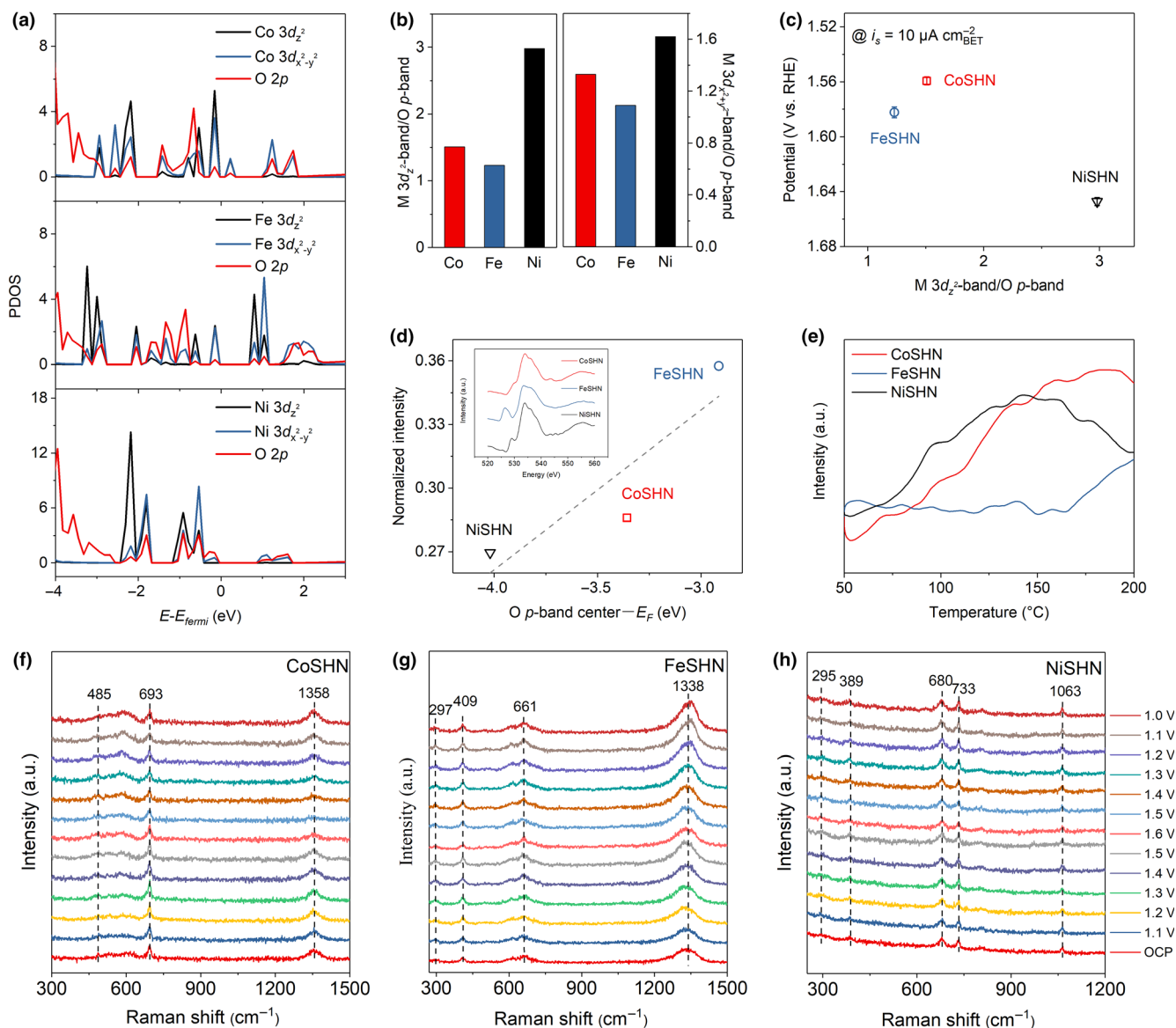
Figure 4. a) PDOS of M $3d_{z^2}$-band, M $3d_{x^2-y^2}$-band, and O p-band. b) The computed $[3d_{z^2}]/[2p]$ and $[3d_{x^2-y^2}/2p]$ ratios of the UMSHNs. c) The iR-corrected potential at 10 $\mu A\ cm^{-2}$ plotted against the $[3d_{z^2}]/[2p]$ ratios of UMSHNs. d) O K-edge XAS data and the normalized intensity of the prepeak versus O p-band center–Fermi level of UMSHNs. e) O_2-TPD pattern of UMSHNs; f–h) in situ Raman spectra.

3. Conclusion

This work develops the design principles for metal silicate hydroxide-based OER electrocatalysts based on the idea that the optimal activity can be obtained by designing materials with moderate covalency of the M–O bonds. The ultrathin nanosheets obtained by surfactant-free hydrothermal synthesis can also be stable. With the e_g filling near unity, the CoSHN exhibits the highest activity outperforming the FeSHN, NiSHN, and the benchmark RuO_2 catalyst. Furthermore, the moderate $[3d_{z^2}/2p]$ and $[3d_{x^2-y^2}/2p]$ ratio is indicative the optimal covalent character of Co–O bond. Both the e_g filling and the $[3d]/[2p]$ ratio correlate with the MOC, so that we conclude that the activity of UMSHNs is governed by the MOC of the active cation and oxygen-containing intermediates, which is further confirmed by O X-edge XAS and O_2-TPD. The

structure durability under oxidation potential further verify the enormous potential of metal silicate hydroxide for OER. This work highlights the importance of tuning surface electronic structure of oxygen electrocatalysts and provides an exciting opportunity and guidelines for the development of efficient metal silicate hydroxide electrocatalysts with the potential for practical utilization in water splitting, rechargeable metal–air batteries, and regenerative fuel cells.

Acknowledgements

Conflict of Interest

The authors declare that they have no conflict of interest.

Supporting Information

Supporting Information is available from the Wiley Online Library or from the author.

Keywords

electrocatalysis, metal silicate hydroxide, metal–oxygen covalency, oxygen evolution reaction, ultrathin nanosheet

References

[1] Z. W. Seh, J. Kibsgaard, C. F. Dickens, I. B. Chorkendorff, J. K. Nørskov, T. F. Jaramillo, *Science* **2017**, *355*, eaad4998.

[2] R. Subbaraman, D. Tripkovic, K.-C. Chang, D. Strmcnik, A. P. Paulikas, P. Hirunsit, M. Chan, J. Greeley, V. Stamenkovic, N. M. Markovic, *Nat. Mater.* **2012**, *11*, 550.

[3] S. Zhao, Y. Wang, J. Dong, C.-T. He, H. Yin, P. An, K. Zhao, X. Zhang, C. Gao, L. Zhang, J. Lv, J. Wang, J. Zhang, A. M. Khattak, N. A. Khan, Z. Wei, J. Zhang, S. Liu, H. Zhao, Z. Tang, *Nat. Energy* **2016**, *1*, 1.

[4] Y. Lee, J. Suntivich, K. J. May, E. E. Perry, Y. Shao-Horn, *J. Phys. Chem. Lett.* **2012**, *3*, 399.

[5] R. R. Rao, M. J. Kolb, N. B. Halck, A. F. Pedersen, A. Mehta, H. You, K. A. Stoerzinger, Z. Feng, H. A. Hansen, H. Zhou, L. Giordano, J. Rossmeisl, T. Vegge, I. Chorkendorff, I. E. L. Stephens, Y. Shao-Horn, *Energy Environ. Sci.* **2017**, *10*, 2626.

[6] F. Song, L. Bai, A. Moysiadou, S. Lee, C. Hu, L. Liardet, X. Hu, *J. Am. Chem. Soc.* **2018**, *140*, 7748.

[7] X. Li, Y. Sun, Q. Wu, H. Liu, W. Gu, X. Wang, Z. Cheng, Z. Fu, Y. Lu, *J. Am. Chem. Soc.* **2019**, *141*, 3121.

[8] H. Fei, J. Dong, Y. Feng, C. S. Allen, C. Wan, B. Volosskiy, M. Li, Z. Zhao, Y. Wang, H. Sun, P. An, W. Chen, Z. Guo, C. Lee, D. Chen, I. Shakir, M. Liu, T. Hu, Y. Li, A. I. Kirkland, X. Duan, Y. Huang, *Nat. Catal.* **2018**, *1*, 63.

[9] S. Zhou, X. Miao, X. Zhao, C. Ma, Y. Qiu, Z. Hu, J. Zhao, L. Shi, J. Zeng, *Nat. Commun.* **2016**, *7*, 11510.

[10] Z. Zhuang, Y. Li, J. Huang, Z. Li, K. Zhao, Y. Zhao, L. Xu, L. Zhou, L. V. Moskaleva, L. Mai, *Sci. Bull.* **2019**, *64*, 617.

[11] J. Suntivich, K. J. May, H. A. Gasteiger, J. B. Goodenough, Y. Shao-Horn, *Science* **2011**, *334*, 1383.

[12] A. Grimaud, K. J. May, C. E. Carlton, Y.-L. Lee, M. Risch, W. T. Hong, J. Zhou, Y. Shao-Horn, *Nat. Commun.* **2013**, *4*, 2439.

[13] T. Wu, S. Sun, J. Song, S. Xi, Y. Du, B. Chen, W. A. Sasangka, H. Liao, C. L. Gan, G. G. Scherer, L. Zeng, H. Wang, H. Li, A. Grimaud, Z. J. Xu, *Nat. Catal.* **2019**, *2*, 763.

[14] Z.-F. Huang, J. Song, Y. Du, S. Xi, S. Dou, J. M. V. Nsanzimana, C. Wang, Z. J. Xu, X. Wang, *Nat. Energy* **2019**, *4*, 329.

[15] N. L. W. Septiani, Y. V. Kaneti, K. B. Fathoni, Y. Guo, Y. Ide, B. Yuliarto, X. Jiang, H. K. Dipojono, D. Golberg, Y. Yamauchi, *J. Mater. Chem. A* **2020**, *8*, 3035.

[16] M. S. Kim, M. H. Naveen, R. Khan, J. H. Bang, *J. Mater. Chem. A* **2020**, *8*, 7647.

[17] B. Wang, C. Tang, H.-F. Wang, X. Chen, R. Cao, Q. Zhang, *J. Energy Chem.* **2019**, *38*, 8.

[18] J. K. Nørskov, J. Rossmeisl, A. Logadottir, L. Lindqvist, J. R. Kitchin, T. Bligaard, H. Jonsson, *J. Phys. Chem. B* **2004**, *108*, 17886.

[19] H. F. Wang, C. Tang, B. Wang, B. Q. Li, Q. Zhang, *Adv. Mater.* **2017**, *29*, 1702327.

[20] C.-X. Zhao, B.-Q. Li, M. Zhao, J.-N. Liu, L.-D. Zhao, X. Chen, Q. Zhang, *Energy Environ. Sci.* **2020**, *13*, 1711.

[21] H.-F. Wang, C. Tang, B.-Q. Li, Q. Zhang, *Inorg. Chem. Front.* **2018**, *5*, 521.

[22] J. Huang, J. Chen, T. Yao, J. He, S. Jiang, Z. Sun, Q. Liu, W. Cheng, F. Hu, Y. Jiang, Z. Pan, S. Wei, *Angew. Chem. Int. Ed. Engl.* **2015**, *54*, 8722.

[23] M. H. Whangbo, H. J. Koo, A. Villesuzanne, M. Pouchard, *Inorg. Chem.* **1920**, *2002*, 41.

[24] C. Qiu, J. Jiang, L. Ai, *ACS Appl. Mater. Interfaces* **2016**, *8*, 945.

[25] J. S. Kim, I. Park, E. S. Jeong, K. Jin, W. M. Seong, G. Yoon, H. Kim, B. Kim, K. T. Nam, K. Kang, *Adv. Mater.* **2017**, *29*, 1606893.

[26] C. Qiu, L. Ai, J. Jiang, A. C. S. Sustain, *Chem. Eng.* **2018**, *6*, 4492.

[27] B. Kim, J. S. Kim, H. Kim, I. Park, W. M. Seong, K. Kang, *J. Mater. Chem. A* **2019**, *7*, 18380.

[28] A. McDonald, B. Scott, G. Villemure, *Micropor. Mesopor. Mat.* **2009**, *120*, 263.

[29] Y. Zhou, S. Sun, J. Song, S. Xi, B. Chen, Y. Du, A. C. Fisher, F. Cheng, X. Wang, H. Zhang, Z. J. Xu, *Adv. Mater.* **2018**, *30*, 1802912.

[30] R. Trujillano, J.-F. Lambert, C. Louis, *J. Phys. Chem. C* **2008**, *112*, 18551.

[31] Y. Yang, L. Dang, M. J. Shearer, H. Sheng, W. Li, J. Chen, P. Xiao, Y. Zhang, R. J. Hamers, S. Jin, *Adv. Energy Mater.* **2018**, *8*, 1703189.

[32] Z. Ye, T. Li, G. Ma, Y. Dong, X. Zhou, *Adv. Funct. Mater.* **2017**, *27*, 1704083.

[33] Y. Peng, Y. Li, Y. Ban, H. Jin, W. Jiao, X. Liu, W. Yang, *Science* **2014**, *346*, 1356.

[34] L. Trotochaud, S. L. Young, J. K. Ranney, S. W. Boettcher, *J. Am. Chem. Soc.* **2014**, *136*, 6744.

[35] S. Sun, H. Li, Z. J. Xu, *Joule* **2018**, *2*, 1024.

[36] K. Jiang, R. B. Sandberg, A. J. Akey, X. Liu, D. C. Bell, J. K. Nørskov, K. Chan, H. Wang, *Nat. Catal.* **2018**, *1*, 111.

[37] Z. Li, Z. Zhuang, F. Lv, H. Zhu, L. Zhou, M. Luo, J. Zhu, Z. Lang, S. Feng, W. Chen, L. Mai, S. Guo, *Adv. Mater.* **2018**, *30*, 1803220.

[38] U. I. Kramm, M. Lefèvre, N. Larouche, D. Schmeisser, J.-P. Dodelet, *J. Am. Chem. Soc.* **2014**, *136*, 978.

[39] C. Wei, Z. Feng, G. G. Scherer, J. Barber, Y. Shao-Horn, Z. J. Xu, *Adv. Mater.* **2017**, *29*, 1606800.

[40] R. L. Frost, S. Bahfenne, J. Čejka, J. Sejkora, J. Plášil, S. J. Palmer, *J. Raman Spectrosc.* **2010**, *41*, 814.

[41] A. Wang, J. J. Freeman, B. L. Jolliff, *J. Raman Spectrosc.* **2015**, *46*, 829.